A&A 484, 241–249 (2008)
DOI: 10.1051/0004-6361:20078001

Astronomy & Astrophysics

The characteristics of the IR emission features in the spectra of Herbig Ae stars: evidence for chemical evolution

C. Boersma[1], J. Bouwman[2], F. Lahuis[3,4], C. van Kerckhoven[5], A. G. G. M. Tielens[1,6], L. B. F. M. Waters[7], and T. Henning[2]

[1] Kapteyn Astronomical Institute, University of Groningen, PO Box 800, 9700 AV, Groningen, The Netherlands
e-mail: boersma@astro.rug.nl
[2] Max-Planck Institut für Astronomie, Königstuhl 17, 69117 Heidelberg, Germany
[3] Space Research Organisation Netherlands, PO Box 800, 9700 AV, Groningen, The Netherlands
[4] Leiden Observatory, PO Box 9513, 2300 RA Leiden, The Netherlands
[5] Instituut voor Sterrenkunde, K. U. Leuven, Celestijnlaan 200B, 3001 Heverlee, Belgium
[6] NASA Ames Research Center, MS 245-3, Moffett Field, CA 94035, USA
[7] Astronomical Institute "Anton Pannekoek", University of Amsterdam, Kruislaan 403, 1098 SJ Amsterdam, The Netherlands

Received 1 June 2007 / Accepted 18 March 2008

ABSTRACT

Context. Infrared (IR) spectra provide a prime tool to study the characteristics of polycyclic aromatic hydrocarbon (PAH) molecules in regions of star formation. Herbig Ae/Be stars are a class of young pre-main sequence stellar objects of intermediate mass. They are known to have varying amounts of natal cloud material still present in their direct vicinity.
Aims. We characterise the IR emission bands, due to fluorescence by PAH molecules, in the spectra of Herbig Ae/Be stars and link observed variations to spatial aspects of the mid-IR emission.
Methods. We analysed two PAH dominated spectra from a sample of 15 Herbig Ae/Be stars observed with the Spitzer Space Telescope.
Results. We derived profiles of the major PAH bands by subtracting appropriate continua. The shape and the measured band characteristics show pronounced variations between the two Spitzer spectra investigated. Those variations parallel those found between three infrared space observatory (ISO) spectra of other, well-studied, Herbig Ae/Be stars. The derived profiles are compared to those from a broad sample of sources, including reflection nebulae, planetary nebulae, H II regions, young stellar objects, evolved stars and galaxies. The Spitzer and ISO spectra exhibit characteristics commonly interpreted respectively as interstellar matter-like (ISM), non-ISM-like, or a combination of the two.
Conclusions. We argue that the PAH emission detected from the sources exhibiting a combination of ISM-like and non-ISM-like characteristics indicates the presence of two dissimilar, spatially separated, PAH families. As the shape of the individual PAH band profiles reflects the composition of the PAH molecules involved, this demonstrates that PAHs in subsequent, evolutionary linked stages of star formation are different from those in the general ISM, implying active chemistry. None of the detected PAH emission can be associated with the (unresolved) disk and is thus associated with the circumstellar (natal) cloud. This implies that chemical changes may already occur in the (collapsing?) natal cloud and not necessarily in the disk.

Key words. stars: planetary systems: formation – infrared: stars – line: profiles – ISM: molecules

1. Introduction

Herbig Ae/Be stars are a class of young stellar objects (Herbig 1960) originally limited to pre-main sequence stars of intermediate mass (2−8 $M_{\odot}$) with spectral class A or B with associated nebulosity and showing emission lines. Over the years, however, the definition has been somewhat relaxed, e.g. the necessity for associated nebulosity (Malfait et al. 1998).

The formation and evolution of isolated, low-mass stars, is relatively well understood (Shu et al. 1987). However, the genesis of intermediate and high-mass stars remains more elusive. For intermediate mass, Herbig Ae/Be stars, it is thought that the formation scheme is more or less a scaled up version of that for low-mass stars. The picture that has thus emerged is that stars form in large molecular clouds and through successive stages of fragmentation, gravitational collapse, and disk accretion, accompanied by bipolar outflows, the star reaches the main sequence. During the later stages of the *pre*-main sequence evolution (0.5−10 Myr), the increased stellar winds from the central object will have removed most of the surrounding molecular cloud material, leaving only the remnant, passive, accretion disk ($R_{\rm disk} \sim 100$AU, $M_{\rm disk} \sim 5.6\times10^{-4}$–$1.5\times10^{-1}$ $M_{\odot}$; Habart et al. 2004; Acke et al. 2004; Waelkens & Waters 1997). This disk – believed to be the site of planet formation – shows up in polarised light and as a strong excess in infrared spectra.

With the 1995 launch of the European Space Agency's Infrared Space Observatory (ESA ISO, Kessler et al. 1996), it became possible for the first time to study the infrared spectrum of Herbig Ae/Be stars in detail. Those studies revealed a large variety in dust composition, both carbonaceous and silicate in nature, and in dust properties (van den Ancker et al. 2000; Bouwman et al. 2000; Waelkens et al. 1996). Specifically, strong infrared (IR) features with satellite features and emission plateaus around 3.3, 6.2, 7.6, 7.8, 8.6, 11.2, and 12.7 micron, associated with polycyclic aromatic hydrocarbons (PAHs), were apparent in many of these objects. PAHs, large molecules of many fused aromatic rings, fluoresce in the infrared upon the

absorption of a single visible or UV photon (Leger & Puget 1984; Cohen et al. 1985; Allamandola et al. 1989). Driven by the dispersal of the disk and the formation of a planetary system, protoplanetary disks are continuously evolving. Geometry, gas, and dust content; gas and dust processing; and transport and mixing are important issues concerning these disks. The diversity of spectral features and their variations within and from source-to-source reflect these issues. However, the interrelationship of the variance in dust composition, the characteristics of the disk, and the global system is not well understood.

Over the years, PAHs have proven to be an ideal probe for many of these properties, e.g., disk geometry (Meeus et al. 2001). The presence of (large) PAH molecules influences many aspects in protoplanetary systems. These aspects include: (surface) chemistry, due to the large surface area of PAHs; heating and cooling through photo-electric ejection; infrared emission; gas-grain collisions; and the charge balance, which in its turn influences the equilibrium state of chemical reactions.

Today, the superior sensitivity of NASA's Spitzer Space Telescope (Werner et al. 2004) allows us to investigate protoplanetary disk systems in better detail than before. Spectra of 15 nearby Herbig Ae/Be stars (Sect. 2), obtained with the Infrared Spectrograph[1] (IRS, Houck et al. 2004), are investigated for emission due to PAHs (Sect. 3). We characterise the individual profiles for the two PAH-dominated spectra found in the sample (Sects. 3.1 and 3.2) and, by using parallels between the morphology of the stellar systems of these sources and those of three well-studied systems, explore possible causes for the observed variations in band profiles (Sect. 4). Similarities between the 6.2 and "7.7" μm band profiles are treated (Sect. 4.1) and the extended nature of the PAH emission is investigated (Sect. 4.2). The origin of the variations in peak position is discussed (Sect. 4.3) and from this, implications about the onset of the chemical modification of PAHs – disk and/or envelope – are inferred (Sect. 4.4). We finish by summarising our findings (Sect. 5).

2. Data

The IRS instrument on board Spitzer was used to obtain the spectra of 36 Herbig Ae/Be (Herbig 1960) stars. We selected the stars from a list of Herbig Ae/Be stars compiled by Malfait et al. (1998) and they complement the 26 Herbig Ae/Be stars observed in the Spitzer guaranteed time observations and legacy programs.

For 15 genuine Herbig Ae/Be stars, we have access to the appropriate wavelength region for detecting emission due to PAHs. Those stars were observed using the short-high and short-low (SH, SL resp.) modules in high accuracy peak-up mode ($\sigma \sim 0.14''$), providing spectra at $R \sim 600$ for the high-resolution module and $R \sim 64-128$ for the low-resolution module, covering wavelengths from 9.9–19.6 and 5.2–14.5 μm for the SH and SL modules, respectively.

The Spitzer Science Center (SSC) processed the data with the science data pipeline version S13.2.0. In order to make more accurate corrections for background emission than possible with the standard pipeline, we adopted the extraction techniques developed by the formation and evolution of protoplanetary systems (FEPS) and cores to disks (C2D) Spitzer legacy teams (Bouwman, in prep.; Lahuis 2007 and c2d-IRS delivery documentation[2]). Extraction of the one-dimensional spectra are done on the intermediate `droopres` and `rsc` products that are provided by the SSC. These data have most of the *Spitzer-specific* artifacts removed. For the `rsc` products this includes straylight and crosstalk corrections, but not flat-fielding. The absolute flux calibration is done using dedicated spectral response functions, derived from IRS spectra of a suite of calibrators using Cohen and MARCS stellar models provided by the SSC.

The high-resolution spectra are extracted from the `rsc` products using an optimal source profile extraction developed by the c2d team. The optimal extraction uses an analytical point spread function (PSF) defined from high S/N sky corrected calibrator data. A simultaneous cross-disperion source profile and extended emission fit is made to the combined dither data. For the extended component, the cross-dispersion profiles of the flat-field images are used. The applied source profile is optimised by comparing the normalised (in cross-dispersion direction) and collapsed (in dispersion/wavelength direction) science source profile with the average profile of the calibrator (point) sources. Bad-pixels are identified and excluded from the profile fits. The optimal extraction allows us to correct the spectrum for local extended emission (see, e.g., Geers et al. 2006; Lahuis et al. 2007), which is crucial in confused regions where the use of separate sky observations is limited.

The low-resolution spectra are extracted from the `droopres` products using a 6.0 pixel fixed-width aperture. Background corrections are made by subtracting the two-dimensional spectral images from the associated nod positions. Besides stray light, this also corrects for anomalous dark current effects. Identified bad pixels are interpolated from the surrounding perimeter. The optimal source extraction is used to derive a possible residual extended emission component in the extraction aperture of the low-resolution order 1 spectra (see Fig. 8). Due to the severe undersampling of the spectral images in the spatial direction, no source profile fits are made for order 2 and 3 and hence no estimate of the extended emission is derived. Flux offsets between orders (particular in the SL module) and modules are apparent. They are probably related to pointing errors and are likely to have introduced low level fringing and small slope changes. For the SL module, we developed a procedure to estimate the pointing errors and correct for them. This procedure minimises the total variance between the flux levels of the individual cycles, nod positions and orders, applying wavelength dependent correction factors to the flux for each relative offset. The procedure simultaneously corrects for fringes. For the high-resolution modules, fringes are removed using the IRSFRINGE package (Lahuis & Boogert 2003). The SMART[3], Higdon et al. (2004) software package has been utilised to further reduce and analyse the data. A mismatch between flux levels of the SL and SH modules is corrected by multiplying the SH flux levels with a constant, which is determined in the overlap region and no adjustment for any differences in tilt for the two sub-spectra is made. As the final reduction steps, outliers are removed and, in regions of spectral overlap, the orders are spliced to form a continuous profile. For rising spectra this splicing may introduce small artifacts in the overlap regions, most notably near 7.5 μm. This is probably related to weak order leakage effects introduced by

[1] The IRS was a collaborative venture between Cornell University and Ball Aerospace Corporation funded by NASA through the Jet Propulsion Laboratory and Ames Research Center.

[2] http://data.spitzer.caltech.edu/popular/c2d/20061201_enhanced_v1/Documents/C2D_Spectr_Expl_Supp.pdf

[3] SMART was developed by the IRS Team at Cornell University and is available through the Spitzer Science Center at Caltech.

Table 1. Overview of the 15 genuine Herbig Ae/Be stars with their dominant spectral component (DC).

Source	DC†	Object	DC†
HD 58647	Si	HD 38120	SP
HD 35929	Si	HD 72106	SP
HD 37258	Si	HD 85567	SP
HD 36917	P	HD 95881	SP
HD 37411	P	HD 142527	SP
HD 36112	SP	HD 190073	SP
HD 37357	SP	HD 244604	SP
HD 37806	SP		

† Si: Silicate dominated, P: PAH dominated, SP: Silicates and PAHs.

the spectral response function, which has been determined using only declining stellar spectra. In the case of extended sources, artifacts may arise due to small differences in aperture size between orders and modules. The relative errors are dominated by the intrinsic (Gaussian) noise in each spectral data point, not by uncertainties in the calibration (Hines et al. 2005). The intrinsic noise is characterised by the deviations found between subsequent nod positions and cycles and are about 2 percent across an order. Between orders it is estimated to be about 5 percent and between modules about 8 percent.

3. Analysis

In order to investigate the emission due to PAHs we roughly classify the spectra of the 15 sources by their dominant spectral component. Table 1 presents our classifications.

To avoid the problem of separating the PAH bands from other dust components, we focus here on the analysis of the two PAH dominated spectra in the sample. In forthcoming papers the spectra dominated by silicate- or with mixed silicate-PAH emission features will be analysed (Bouwman et al., in prep.).

The Herbig Ae/Be stars associated with these two spectra are HD 36917 and HD 37411. Both stars are located south of the Orion belt in the OB1c association, of which HD 36917 is a spectroscopic binary (Levato & Abt 1976). The shape of its SED, with its drop between 2–20 μm and rise beyond 20 μm, suggest a cleared (inner) region in its circum-stellar disk (planet?). The star HD 37411 is a visual binary, showing no emission lines. The optical spectrum of the binary indicates a late type (K-M) companion (Van den Ancker, unpublished). Table 2 summarises the astrometric data and Table 3 the available IRS data. Figure 1 presents the fully reduced Spitzer SL and SH spectra.

In order to derive the individual PAH profiles, a continuum is established. To facilitate comparison with previous studies we adopt the procedures as outlined by Peeters et al. (2002), van Diedenhoven et al. (2004), and Hony et al. (2001), assuming PAHs are not significantly contributing to the continuum. In accordance with these procedures, the continuum for the 6.2 μm region is approximated by a single spline; for the 7–9 μm region a general continuum and an additional plateau component are defined, where the general continuum is approximated by a single spline, with points selected between 5–6 μm, 9–10 μm and near 7 μm. With additional points near 8.3 μm the plateau component is fixed. The continuum in the 11.2 μm region is approximated by a single spline. Points between 9–10.5, 14.5–15.5 and near 11.8 and 13.1 μm are selected to define a single spline to approximate the continuum in the 12 μm region.

3.1. Results

Table 4 summarises the identified PAH bands and plateaus in the continuum subtracted spectra. The spectra of the two sources show all of the well-known IR emission features at 6.2, 7.7, 8.6, and 11.2 μm and, in addition, in some sources, the weak bands at 5.25, 5.7, 6.0, 12.0, 12.7, and 16.4 μm and the broad plateaus underneath the 6.2, 7.7, and 15 μm regions. Table 5 presents the spectral properties of the major PAH bands. These properties were determined fitting a single Gaussian to the band.

Apart from PAH band emission also other, dust and non-dust components are identified. For instance, the aliphatic hydrocarbon features at 6.85 and 7.25 μm (Sloan et al. 2005, and refs therein) in the SL spectra and the Ne II, H_2 S(1) and S III lines at, respectively, 12.8, 17.1, and 18.7 μm in the SH spectra of HD 36917. Between 9.0–13 μm, a broad emission component, reminiscent of warm silicate dust, is visible, particularly in HD 37411. In our analyses of the emission feature around 11 μm we subtracted this component using a spline fit (see Fig. 4).

3.2. Profiles

The apparent variations in peak position, width and wing shapes between the derived profiles is much larger than could be caused by the uncertainty in the adopted continuum. Studies of the detailed profiles of the PAH bands in the ISO SWS spectra of a large sample of stellar sources, planetary nebulae (PNe), reflection nebulae, H II regions and galaxies have revealed that the bands in the 6–9 μm range show strong variation in peak position and profile (Peeters et al. 2002). Those studies showed that the variations in the PAH bands correlate with object type. All ISM-like sources belong to group A characterised by a "6.2 μm" band peaking at 6.2 μm and a 7.7 μm band peaking at 7.6 μm, and while the isolated Herbig Ae/Be stars, along with a few post-AGB stars and most PNe, belong to group B, which are characterised by a "6.2" μm band peaking around 6.28 μm and a 7.7 μm band peaking at 7.9 μm. Finally, two post-AGB stars make up group C, characterised by a "6.2" μm band peaking at 6.3 μm and with no apparent 7.7 μm band, but a broad "8.22" μm feature (Figs. 2–4; Table 6). In van Diedenhoven et al. (2004), the variations in the 3.3 and 11.2 μm bands are studied. However, the observed variation are shown to be more modest and the object correlation not as tight than those observed for the 6–9 μm region.

The observed diversity in peak position, profile, and relative strength of the PAH bands are ascribed to global changes in the physical and chemical characteristics of the emitting PAH family. More specifically, variations in the peak positions of the 6.2 μm band are thought to indicate incorporation of nitrogen in the aromatic ring structure (Peeters et al. 2002; Bauschlicher 2002). The 7.6/7.8 μm bands are also likely to be related to chemical modifications, based on the strong correlation with the 6.2 μm variations. In contrast, variations in the ratio of the C-H modes to the C-C modes (e.g., 11.2/6.2 μm) are attributed to variations in the charge state of the emitting PAH molecules (Allamandola et al. 1999; Hony et al. 2001; Bakes et al. 2001). Emission between 10.9 and 11.1 μm is attributed to the out-of-plane bending vibrations of solo-CH groups on the periphery of moderately sized (~100 carbon atoms) PAHs (Hudgins & Allamandola 1999). In Figs. 2–4, the derived profiles from the two Spitzer sources are compared to the characteristic profiles from Peeters et al. (2002) and van Diedenhoven et al. (2004).

In Fig. 2, the 6.2 μm profiles are compared. The 6.2 μm profile of HD 36917 resemblances that of class A best and for

Table 2. Astrometric data for HD 36917 and HD 37411.

Object	α [2000]	δ [2000]	Region	d[pc]	Ref.	Sp. Type	Ref.	A_V[mag]
HD 36917	05h34m46.98s	–05d34m14.6s	Orion OB1c	510	1	B9.5V + A0V	2	0.49
HD 37411	05h38m14.51s	–05d25m13.3s	Orion OB1c	510	1	A0 + K-M	3	0.00

1: de Zeeuw et al. (1999); 2: Levato & Abt (1976); 3: Gray & Corbally (1998).

Table 3. Available IRS data on HD 36917 and HD 37411.

	Module				
Object	SL[1]	SH[1]	LH[1]	PU-blue[2]	#[3]
HD 36917	√ (2)	√ (2)	√ (3)		18
HD 37411	√ (2)	√ (3)	√ (4)	√	22

1: Number of cycles in parentheses; 2: peak-up blue image (13.5−18.7 μm); 3: total number of spectra.

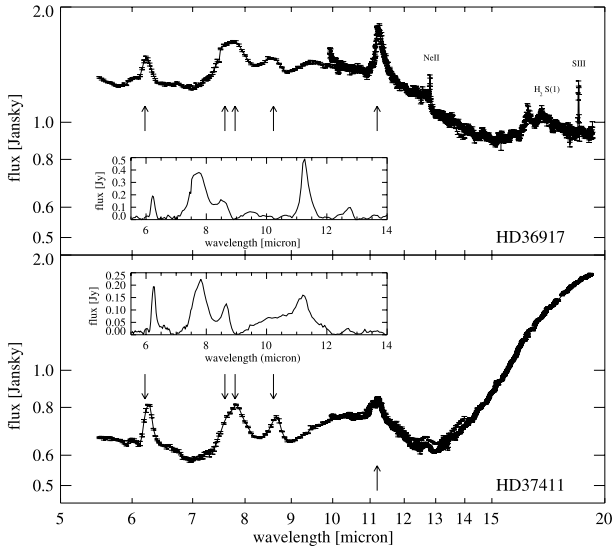

Fig. 1. Fully-reduced SL and SH spectra for HD 36917 and HD 37411. The arrows indicate the positions of the PAH bands of interest. The inset displays the residual (SL) spectrum when approximating the continuum with a single spline.

HD 37411 that of class B. The profiles in both classes show a variation in the strength of the red tail, relative to the peak. In that respect the red tails of both sources fall off more rapidly than the characteristic profile that defines their class, but it is known to vary (Peeters et al. 2002).

The variations in the "7.7" μm feature (Fig. 3) are particular interesting. Remarkably, HD 36917 is best seen as a *blend* of a class A and class B profile. The "7.7" μm band in the spectrum of HD 37411 is a clear class B profile.

The differences between the 11.2 μm profiles are subtle and difficult to discern, despite the high-resolution profiles (Fig. 4). Again, HD 36917 shows evidence for a blend of a class A and class B profile. The classification for HD 37411 is hampered by the dominating continuum component between 9−13 μm (inset Fig. 1). As described in Sect. 3.1, this additional component has been approximated by a single spline and has been subtracted. The result is presented in Fig. 4

Both spectra show evidence for a 11.1 μm feature. Many sources show this weak "satellite" accompanying the 11.2 μm feature (Hony et al. 2001). However, the 11.1 μm feature in HD 37411 is very strong relative to the 11.2 μm band. This spectral region is often confused by emission bands due to forsterite. In astronomical spectra, these often coincide with the 11.2 μm band. However, we note that laboratory spectra show evidence for forsterite near 11.0 μm (Tamanai et al. 2006). The broad 10 μm band, evident in Fig. 1, indicates the presence of warm silicate in the source and supports this suggestion. In any case, focussing on the PAHs and guided by the high-resolution data, the profile is classified A. Table 7 summarises the assigned classes.

4. Discussion

Sloan et al. (2007) have identified systematic variations in the peak position of the 7.7 and 11.2 μm band with the spectral type of the exciting star. We also recognise such variations in the spectra of HD 36917 and HD 37411. We note that both stars have similar spectral type (~B9). Going back to ISO SWS (de Graauw et al. 1996) data (Van Kerckhoven 2002) we have retrieved additional spectra of three well-studied and well-characterised Herbig Ae/Be stars, which provide additional insight in the possible factors driving these spectral variations.

The first star is TY CrA, a double-lined eclipsing binary consisting of a Herbig Ae/Be object (Thé et al. 1994), close to the zero age main sequence, and a late-type pre-main-sequence object. The object is located near one of the densest parts of the R Corona Australis star-forming region, embedded in the bright reflection nebula NGC 6726/6727 (Harju et al. 1993). The infrared emission seen in the ISO spectrum does not originate from TY CrA itself, but from the nearby "TY CrA bar" (Siebenmorgen et al. 2000; Geers et al. 2007). The second star is HD 97048, it is located in the Chamaeleon I cloud of the Chamaeleon T association, which illuminates the bright reflection nebula Ced 111. Spatial studies on the PAH emission done with the VLT's spectrometer and imager for the mid-infrared (VISIR; Lagage et al. 2004) and ISO have revealed a circumstellar (~0.5″) and a more extended component (>5.4″; Prusti et al. 1994; Siebenmorgen et al. 2000; van Boekel et al. 2004; Habart et al. 2006). Finally, HD 100546 is a typical isolated Herbig Ae/Be star, which has no companions within 1500 AU and is not associated with the nearby dark cloud DC 292.6-7.9 (Grady et al. 2001). The mid-IR emission of this source clearly originates from the circumstellar protoplanetary disk, which has a gap of about ~10 AU with a "puffed-up" inner rim (Acke & van den Ancker 2006).

4.1. The profiles

Figure 5 compares the "7.7" μm feature profiles[4] of all five sources. The peak position of the 7.7 μm feature varies considerably in this sample from 7.6 μm all the way to 8.0 μm. Most striking is that the profile for HD 97048 can be obtained by combining the profiles from TY CrA and HD 100546 (Van Kerckhoven 2002). The two *Spitzer* sources show similar behaviour. Indeed, the 7.7 μm feature of HD 36917 may be obtained by combining the class B profile of HD 37411 with a class A-like profile (labeled *pseudo*) in Fig. 5.

[4] For details concerning the ISO SWS spectra, such as data reduction and analyses we refer to Van Kerckhoven (2002).

Table 4. Detected PAH band components in HD 36917 and HD 37411.

Source	5.25	5.7	6.0	6.2	7.6/7.8	8.6	11.0	11.2	12.0	12.7	13.5	16.4	Plateau
HD 36917	√	√	√	√	√	√		√	√	√	√	√	√
HD 37411	√		√	√	√	√	?	√	?	√			

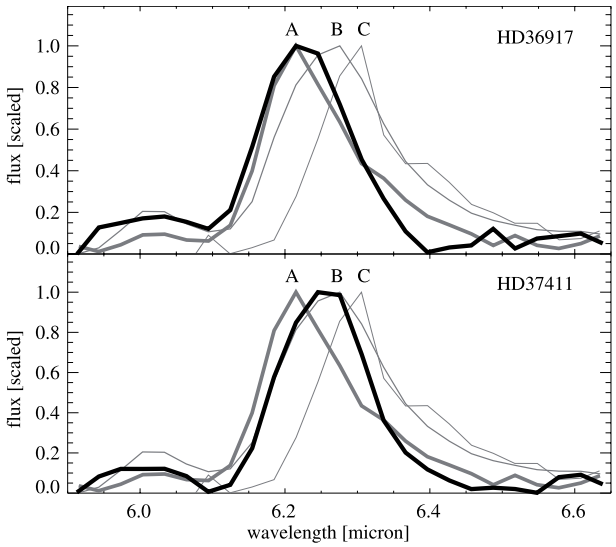

Fig. 2. The derived 6.2 μm profiles (black) after subtraction of the underlying continuum. For comparison, the three characteristic profiles derived in the study by Peeters et al. (2002) are shown at matched resolution in grey.

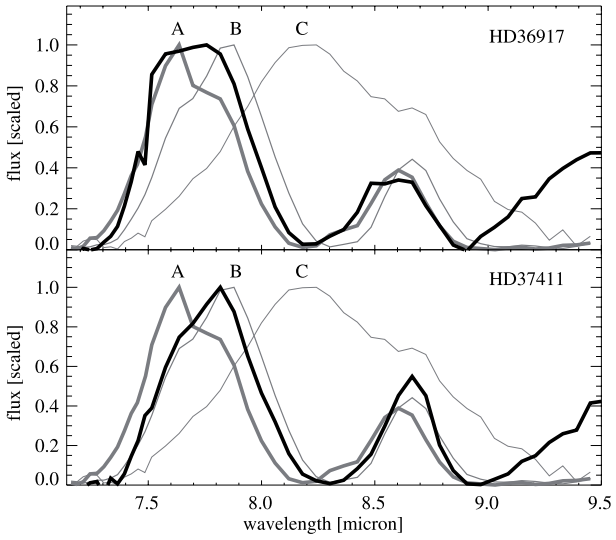

Fig. 3. The derived "7.7" μm profiles (black) after subtraction of the underlying continuum. For comparison, the three characteristic profiles derived in the study by Peeters et al. (2002) are shown at matched resolution in grey.

Table 7 shows that the systematic differences between the profiles of the three *ISO* sources are also analog to those between the profiles of the two *Spitzer* sources. The spectral type of the five sources are similar (~B9), therefore, the variations in the derived profiles between these stars cannot be caused by differences in the exciting spectrum.

Sloan et al. (2007) find a correlation between the central wavelength of the 7–8 μm feature and the effective temperature of the exciting star. We have determined the peak position of the 7–8 μm band for the 2 *Spitzer* and 3 *ISO* sources in our study in the same manner as Sloan et al. (2007) and plotted our results with the data from Sloan et al. (2005, 2007) in Fig. 6. Although there is no clear break in the correlation, a jump is discernible around 10 000 Kelvin. Following Sloan et al. (2007), the diagram is interpreted to reveal a "7.7" μm band peaking at 7.6 μm (class A) for $T_{\rm eff} \gtrsim 10\,000$ K, at 7.9 μm (class B) for $10\,000 \gtrsim T_{\rm eff} \gtrsim 7000$ K and at 8.2 μm (class C) for $T_{\rm eff} \lesssim 7000$ K. We note that this subdivision parallels a subdivision in source classification as with class A containing sources dominated by ISM material, class B comprising Herbig stars, and class C consisting of post-AGB objects. We point out that in this sample objects, like the PNe NGC 7027, with $T_{\rm eff} \simeq 200\,000$ K and belonging to *class B*, are not shown.

Table 5. Spectral properties of the major PAH bands.

		HD 36917	HD 37411
6.2	position[1]	6.22	6.25
	FWHM[1]	0.27	0.15
	EW[2]	0.028	0.049
	F[3]	2.7	2.37
7.7	position	7.63	7.78
	FWHM	0.42	0.43
	EW	0.092	0.12
	F	6.3	3.63
8.6	position	8.58	8.64
	FWHM	0.33	0.25
	EW	0.022	0.036
	F	1.26	0.97
11.2	position	11.29	11.21
	FWHM	0.31	0.38
	EW	0.12	0.053
	F	3.74	0.94
11.2[4]	position	11.32	11.22
	FWHM	0.42	0.29
	EW	0.11	0.063
	F	4.4	1.1
12.7	peak	12.72	12.71
	FWHM	0.34	0.33
	EW	0.026	0.013
	F	0.67	0.16

1: [μm]; 2: equivalent width: $\int$[(band − continuum)/continuum]dλ; 3: [$10^{-15} \cdot$ W $\cdot$ m^{-2}]; 4: Hi-res profile.

4.2. Extended PAH band emission

Van Kerckhoven (2002) and Peeters et al. (2003) note that the observed variations in the 7–9 μm region might well be due to differences in morphology of the sources, combining ISM material and/or disks. Most resounding in this respect is the source HD 97048, which morphologically consists of a spatial combination of circumstellar disk material and interstellar material

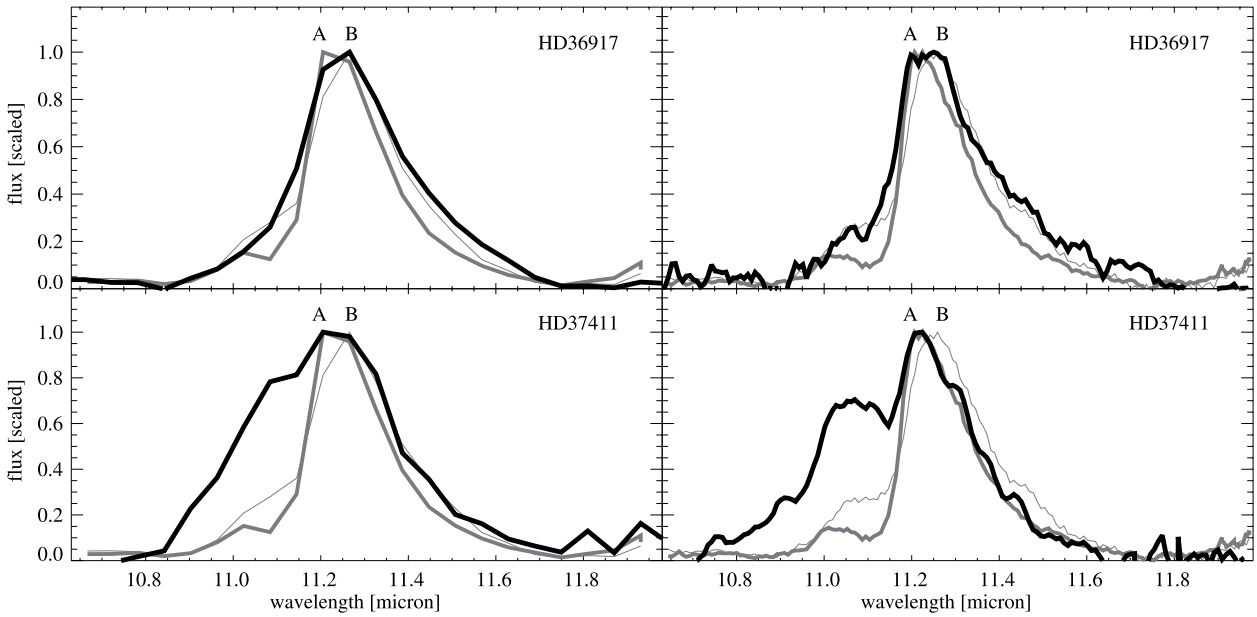

Fig. 4. The derived 11.2 μm profiles (black) after subtraction of the underlying continuum and correction for the broad 10 μm feature in HD 37411. For comparison, the two characteristic profiles derived in the study by van Diedenhoven et al. (2004) are shown at matched resolution in grey. *Left*: the derived low-resolution (SL) profiles. *Right*: the derived high-resolution (SH) profiles.

Table 6. The spectral characteristics for the classes from Peeters et al. (2002) and van Diedenhoven et al. (2004). λ_x indicates the peak positions, in μm.

The 5–9 μm region				
Class	Object	$\lambda_{6.2}$	$\lambda_{7.7}$[1]	$\lambda_{8.6}$
$\mathcal{A}$	ISM-like	~6.22	7.6/equal	~8.6
$\mathcal{B}$	non-ISM-like	6.24–6.28	"7.8"	>8.62
C	non-ISM-like	~6.3	8.22	none
The 11.2 μm region				
Class	Object	$\lambda_{11.2}$	$FWHM_{11.2}$	
$A_{11.2}$	ISM-like	~11.20–11.24	~0.17	
$A(B)_{11.2}$	uncorrelated	~11.20–11.24	~0.21	
$B_{11.2}$	uncorrelated	~11.25	~0.20	

1: The "7.7" μm feature is classified by its dominant component, the 7.6 and/or the 7.8 μm component.

Table 7. Assigned classes, see text for details.

	6.2	7.7	11.2
HD 36917	A	A + B	B (+ A?)
HD 37411	B	B	A
TY CrA	A	A	A
HD 97048	A	A + B	A
HD 100546	B	B	–[1]

1: Due to strong silicate contamination, classification of the 11.2 μm profile has been omitted.

(Lagage et al. 2004) and spectroscopically combines characteristics of classes A and B.

Linking back to the two *Spitzer* sources, this connects the detected PAH emission from HD 37411 to the circumstellar disk and, particularly fascinating, the PAH emission from HD 36917 to, in part, the surrounding cloud and/or envelope (pseudo source) and, in part, the circumstellar disk. Intrigued by the notion of two different, spatially, separated PAH families in HD 36917, we are motivated to investigate the *spatial* variation of the PAH emission coming from HD 36917.

The available 8 μm IRAC (Fazio et al. 2004) mosaic from part of the OB1c association is presented in Fig. 7. The image is centred on the position of HD 36917 and the colour scaling is chosen to emphasise the emission from the envelope. The strong and rich morphology of the infrared background is clearly visible. The IRAC data suggest diffuse extended nebulosity associated with the source on scales up to at least ~1′ (3×10^4 AU).

Figure 8 illustrates the use of the source profile extraction to decompose both spatial components (see Sect. 2). In the left panel, part of the first order in the SL module of the spectral image of HD 36917 is shown, demonstrating the extended nature of the 11.2 and 12.7 μm PAH bands in HD 36917. The panel in the middle displays the result (black) of simultaneous fitting a source profile and a 2nd order polynomial (red) to the combined dither data (grey). A 2nd order polynomial for the extended emission produces the optimal extraction, providing a reasonable approximation to the observed emission. A higher order polynomial results in increased noise, while a lower order polynomial provides an inferior fit and underestimates the extended emission component. The half-width of the extended emission is about 6 pixels (≃11″; 6×10^3 AU). The panel to the right in Fig. 8 shows the cross-dispersion profile from 11.2 to 11.5 μm (black) compared with the calibration profile derived from standard stars (grey). In Fig. 9, the SL and SH spectra, corrected for local background emission, are presented.

Remarkably, in both the SL and SH spectra the PAH signatures have largely disappeared. As expected, this procedure removes the forbidden atomic lines in the SH spectrum. In addition, the 11.2, and 12.7 μm band and the plateau underneath 16.4 μm have vanished. Obviously, the red end of the "7.7" μm feature, the 11.2 and 12.7 μm PAH band emission originates from the surrounding cloud/envelope. It is clear that in this source there is *no* evidence for PAH emission associated with the direct (unresolved) circumstellar disk (~0.2″; $R \sim 50$ AU).

Note that, in contrast to the PAH features, the 16.4 μm band seems to be associated with the direct circumstellar environment of the star. Although the band is located in a region where two orders overlap (12 and 13) and, therefore, the extended

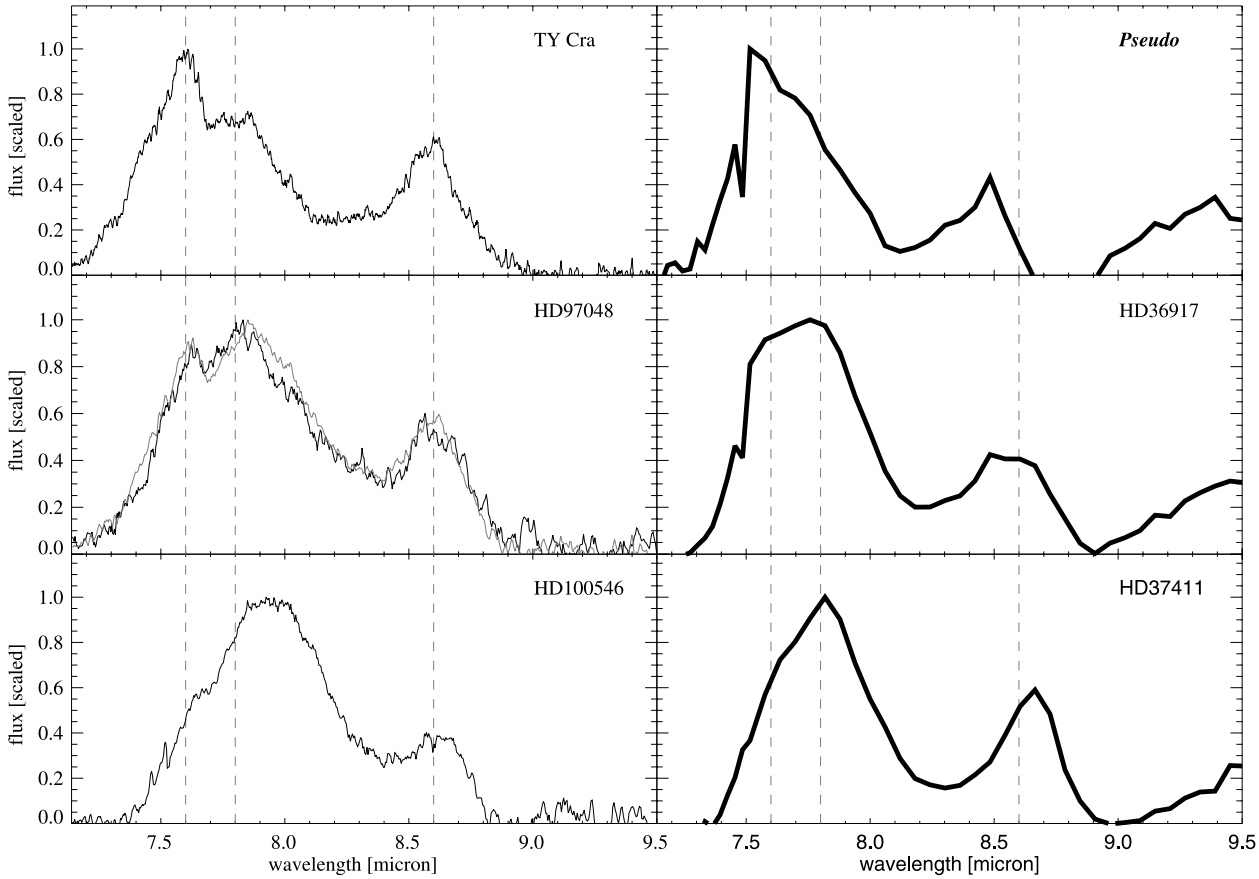

Fig. 5. *Left*: the normalised profiles of the "7.7" μm feature of HD 97048, TY CrA, and HD 100546, as obtained by the SWS instrument on board ISO. The dashed lines indicate the peak positions of the major PAH band components. In grey the combined profile for HD 97048, constructed from TY CrA and HD 100546, is presented. Note the quality of the match. *Right*: the normalised profiles of the "7.7" μm feature of HD 36917 and HD 37411, as obtained by the IRS instrument on board Spitzer. The profile labled *pseudo* is obtained by subtracting the profile of HD 37411 from that of HD 36917. The dashed lines indicate the peak positions of the major PAH band components.

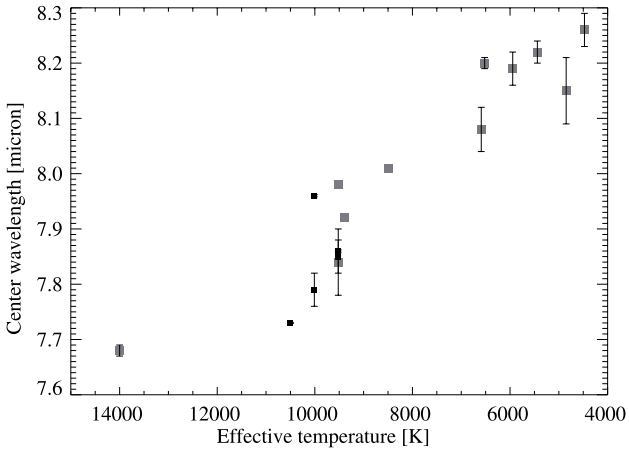

Fig. 6. Correlation between the central wavelength of the 7−8 μm band and the effective temperature of the exciting star. The 5 Herbig stars used in this study are shown as black squares. Adopted from Sloan et al. (2007).

emission estimate is somewhat more uncertain, forsterite does show some weak features near this position (Koike et al. 2003, 16.3 μm). This actually suggests the presence of processed silicate material in the disk. Furthermore, spectral structure between 10.5−10.9 μm appears in the background corrected spectra, most distinctly seen in the SL spectrum. This could be the weak PAH band first recognised by Witteborn et al. (1989) and later, e.g., Beintema et al. (1996).

The absence of PAH features in the spectra of the disk is not too surprising. Meeus et al. (2001) classified 46 spectra of Herbig Ae/Be stars, based on the shape of the SED in the mid-IR, in distinctive groups. Their group I sources all showed emission due to PAHs, but their group II sources show no or only weak PAH emission. They link this difference to the geometry of the circumstellar disk; flaring vs. self-shadowed. The SED of HD 36917 makes it a Group II source (Habart et al. 2004), consistent with this interpretation.

The PAH emission in HD 36917 originates from a region 6×10^3 AU in size and, therefore, is likely associated with an extended envelope rather than a disk. Thus, although the spectra show evidence for a "processed" PAH component peaking toward the source – thus associated with the source – the processing itself seems to occur on a scale-size, which is much larger than a star/disk system. Therefore, it has the appearance that the spectral variations can be attributed to the spatial structure of the region, although division into a clear disk and cloud component is not evident from our data.

4.3. Origin of the variations

The observed trend between the central wavelength of the 7.7−7.9 μm feature and the spectral type of the irradiation star, as shown in Fig. 6, shows a jump near 10 000 Kelvin. The spectral

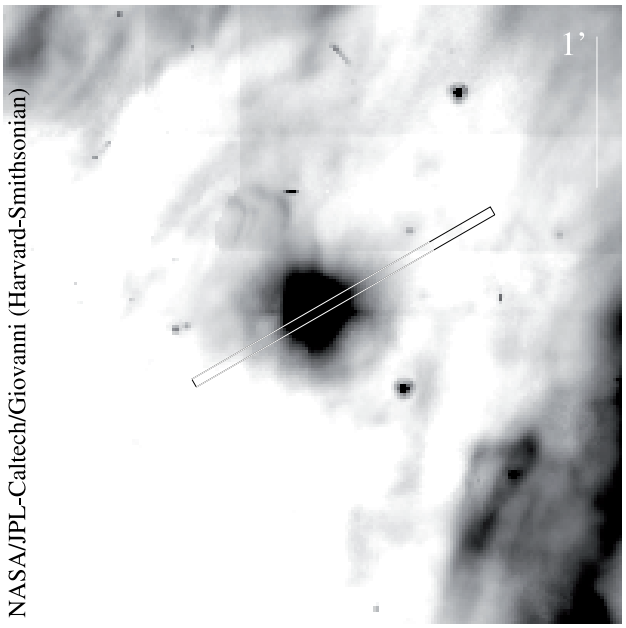

Fig. 7. 8 μm IRAC mosaic from part of the OB1c association, centred on HD 36917 and the colour scaling is chosen to emphasise the emission coming from the envelope. Also shown is the IRS SL slit on the source.

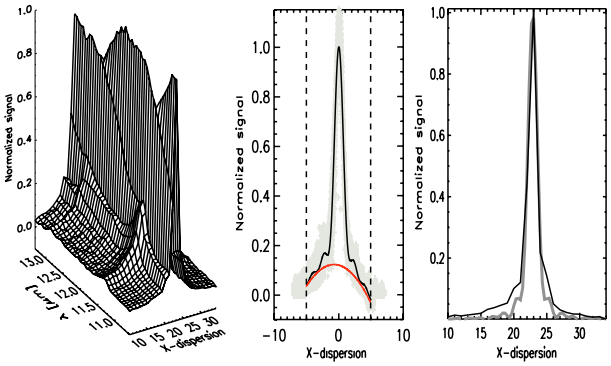

Fig. 8. *Left*: the normalised source profile of a section from the SL1 long-slit 2-D spectral image as observed toward HD 36917. As a result of the angle of the order across the image, the profile centre moves in cross-dispersion. This results in a changing distribution of the profile signal across pixels, hence the apparent lower than unity profile at certain wavelengths. The presence of a spatially extended component near the 11.2 and 12.7 μm PAH bands in HD 36917 is clearly visible. *Middle*: the simultaneous fit (black) of a source profile and a 2nd order polynomial to the combined dither data (grey). *Right*: the average cross-dispersion profile from 11.2 to 11.5 μm is compared with the calibration profile derived from the standard stars. For the extraction the calibration cross-dispersion profile is fit in combination with a 2nd order polynomial to decompose the spatial components.

variations in the "7.7" μm feature reflect chemical modifications and Sloan et al. (2007) suggested that these modifications are likely driven by UV processing. But hot class B sources, such as NGC 7027, seem to indicate that other source characteristics, besides effective temperature, may be of importance too. Such characteristics could include local density or history of the carriers. Now, the jump near 10 000 Kelvin seems to indicate that for Herbig Ae stars these other factors are of consequence. In this study the spectral variations are linked to PAHs in spatial structures, promoting differences in UV processing. Note that the extended nature of HD 36917 lends itself particularly well to a spatial-spectral study and may well settle the factors involved in the chemical processing of PAHs.

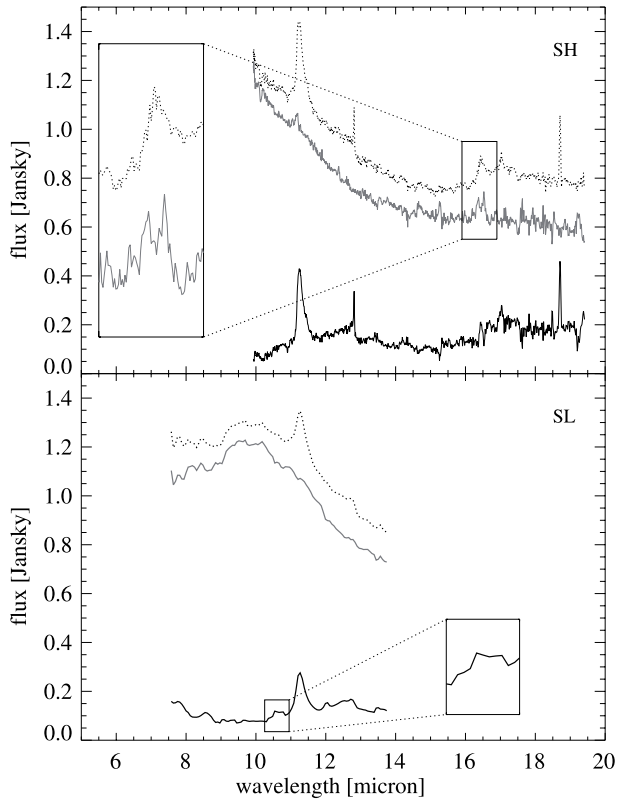

Fig. 9. The local background corrected SL (*bottom*) and SH (*top*) spectra for HD 36917, as obtained with the decomposition. The corrected spectra are grey, the uncorrected spectra are dotted grey and the background estimates are black. The boxes show a few interesting spectral regions.

4.4. Implications

The chemical modifications driving the observed variations in Herbig Ae stars may well be due to a transition from stable aromatic structures in the cloud (class A), to more labile aliphatic-like structures in the circumstellar environment (class B) (Sloan et al. 2007). However, whereas post-AGB objects (class C) and ISM sources (class A) lend themselves to an evolutionary interpretation – from labile aliphatic hydrocarbons in the benign conditions of post-AGB objects to stable aromatic hydrocarbons in the harsh environment of the ISM – it would be unlikely for the aromatic structures to regenerate their aliphatic side-groups when going from the ISM to the protoplanetary disks. Rather, we interpret the observed spectral variations as reflecting the presence of an active chemical balance – in *all* sources – between hydrogenation, carbon reactions building (aliphatic) hydrocarbons, and UV photons breaking them down.

5. Summary and conclusions

From a sample of 15 Herbig Ae/Be stars we analysed the two PAH dominated *Spitzer* IRS spectra. The derived profiles have been classified according the scheme of Peeters et al. (2002). Comparison of these profiles with profiles obtained using *ISO*'s SWS from three (spatially) well studied objects indicate the presence of two dissimilar, spatially separated, PAH families for HD 36917.

The analysis presented here shows again, based on the variation in band profiles, that PAHs in subsequent, evolutionary linked stages of star formation, are different from those in the general ISM (Hony et al. 2001). While previously the required chemical processing of the PAHs was placed in the protoplanetary disk phase (Van Kerckhoven 2002; Peeters et al. 2003), the evidence presented here, shows that such chemical changes may already occur in the (collapsing?) natal cloud. The supporting evidence for this is that the detected PAH emission cannot be associated with the (unresolved) disk and must thus be associated with the circumstellar (natal) cloud. Furthermore, the presence of the two distinct PAH families suggests active chemistry. Further studies on the spatial and spectral variations in the PAH spectra of these sources may be helpful to disentangle the factors that stimulate the processing of PAH molecules.

Future observation, using (high-resolution) spectral mapping techniques, should provide a better handle on the spatial variations of the PAH emission/profiles coming from and surrounding HD 36917 and possibly link them to the changing radiation field as one moves out from the central star. Additional laboratory studies are required to explain the transition from class A PAH profiles in the circumstellar (natal) cloud to class B profiles in disks.

Acknowledgements. We gratefully thank Els Peeters for providing the ISO SWS data and acknowledge Mario van den Ancker for providing a literature overview on the Herbig Ae/Be stars investigated.

References

Acke, B., & van den Ancker, M. E. 2006, A&A, 449, 267
Acke, B., van den Ancker, M. E., Dullemond, C. P., van Boekel, R., & Waters, L. B. F. M. 2004, A&A, 422, 621
Allamandola, L. J., Tielens, G. G. M., & Barker, J. R. 1989, ApJS, 71, 733
Allamandola, L. J., Hudgins, D. M., Bauschlicher, C. W., & Langhoff, S. R. 1999, A&A, 352, 659
Bakes, E. L. O., Tielens, A. G. G. M., & Bauschlicher, C. W. 2001, ApJ, 556, 501
Bauschlicher, C. W. 2002, ApJ, 564, 782
Beintema, D. A., van den Ancker, M. E., Molster, F. J., et al. 1996, A&A, 315, L369
Bouwman, J., de Koter, A., van den Ancker, M. E., & Waters, L. B. F. M. 2000, A&A, 360, 213
Cohen, M., Tielens, A. G. G. M., & Allamandola, L. J. 1985, ApJ, 299, L93
de Graauw, T., Haser, L. N., Beintema, D. A., et al. 1996, A&A, 315, L49
de Zeeuw, P. T., Hoogerwerf, R., de Bruijne, J. H. J., Brown, A. G. A., & Blaauw, A. 1999, AJ, 117, 354
Fazio, G. G., Hora, J. L., Allen, L. E., et al. 2004, ApJS, 154, 10
Geers, V. C., Augereau, J.-C., Pontoppidan, K. M., et al. 2006, A&A, 459, 545
Geers, V. C., van Dishoeck, E. F., Visser, R., et al. 2007, A&A, 476, 279
Grady, C. A., Polomski, E. F., Henning, T., et al. 2001, AJ, 122, 3396
Gray, R. O., & Corbally, C. J. 1998, AJ, 116, 2530
Habart, E., Natta, A., & Krügel, E. 2004, A&A, 427, 179
Habart, E., Natta, A., Testi, L., & Carbillet, M. 2006, A&A, 449, 1067
Harju, J., Haikala, L. K., Mattila, K., et al. 1993, A&A, 278, 569
Herbig, G. H. 1960, ApJS, 4, 337
Higdon, S. J. U., Devost, D., Higdon, J. L., et al. 2004, PASP, 116, 975
Hines, D. C., Carpenter, J. M., Bouwman, J., et al. 2005, FEPS Data Explanatory Supplement, Version 3.0 (Pasadena: SSC)
Hony, S., Van Kerckhoven, C., Peeters, E., et al. 2001, A&A, 370, 1030
Houck, J. R., Roellig, T. L., van Cleve, J., et al. 2004, ApJS, 154, 18
Hudgins, D. M., & Allamandola, L. J. 1999, ApJ, 516, L41
Kessler, M. F., Steinz, J. A., Anderegg, M. E., et al. 1996, A&A, 315, L27
Koike, C., Chihara, H., Tsuchiyama, A., et al. 2003, A&A, 399, 1101
Lagage, P. O., Pel, J. W., Authier, M., et al. 2004, The Messenger, 117, 12
Lahuis, F. 2007, Ph.D. Thesis, Leiden Observatory, Leiden University, PO Box 9513, 2300 RA Leiden, The Netherlands
Lahuis, F., & Boogert, A. 2003, in SFChem 2002: Chemistry as a Diagnostic of Star Formation, proceedings of a conference held August 21–23, 2002 at University of Waterloo, Waterloo, Ontario, Canada N2L 3G1, ed. C. L. Curry, & M. Fich (Canada, Ottawa: NRC Press), 335
Lahuis, F., van Dishoeck, E. F., Blake, G. A., et al. 2007, ApJ, 665, 492
Leger, A., & Puget, J. L. 1984, A&A, 137, L5
Levato, H., & Abt, H. A. 1976, PASP, 88, 712
Malfait, K., Bogaert, E., & Waelkens, C. 1998, A&A, 331, 211
Meeus, G., Waters, L. B. F. M., Bouwman, J., et al. 2001, A&A, 365, 476
Peeters, E., Hony, S., Van Kerckhoven, C., et al. 2002, A&A, 390, 1089
Peeters, E., van Diedenhoven, B., Van Kerckhoven, C., et al. 2003, in Astrophysics of Dust
Prusti, T., Natta, A., & Palla, F. 1994, A&A, 292, 593
Shu, F. H., Adams, F. C., & Lizano, S. 1987, ARA&A, 25, 23
Siebenmorgen, R., Prusti, T., Natta, A., & Müller, T. G. 2000, A&A, 361, 258
Sloan, G. C., Keller, L. D., Forrest, W. J., et al. 2005, ApJ, 632, 956
Sloan, G. C., Jura, M., Duley, W. W., et al. 2007, ApJ, 664, 1144
Tamanai, A., Mutschke, H., Blum, J., & Meeus, G. 2006, ApJ, 648, L147
Thé, P. S., de Winter, D., & Perez, M. R. 1994, A&AS, 104, 315
van Boekel, R., Waters, L. B. F. M., Dominik, C., et al. 2004, A&A, 418, 177
van den Ancker, M. E., Bouwman, J., Wesselius, P. R., et al. 2000, A&A, 357, 325
van Diedenhoven, B., Peeters, E., Van Kerckhoven, C., et al. 2004, ApJ, 611, 928
Van Kerckhoven, C. 2002, Ph.D. Thesis, Instituut voor Sterrenkunde, Katholieke universiteit Leuven
Waelkens, C., & Waters, L. B. F. M. 1997, in Infrared Space Interferometry: Astrophysics & the Study of Earth-like Planets, ed. C. Eiroa et al., 119
Waelkens, C., Waters, L. B. F. M., de Graauw, M. S., et al. 1996, A&A, 315, L245
Werner, M. W., Roellig, T. L., Low, F. J., et al. 2004, ApJS, 154, 1
Witteborn, F. C., Sandford, S. A., Bregman, J. D., et al. 1989, ApJ, 341, 270